



# Comparable investigation of unsupported MoS<sub>2</sub> hydrodesulfurization catalysts prepared by different techniques: Advantages of support leaching method



A.N. Varakin<sup>a</sup>, A.V. Mozhaev<sup>a</sup>, A.A. Pimerzin<sup>a</sup>, P.A. Nikulshin<sup>a,b,\*</sup>

<sup>a</sup> Samara State Technical University, 244, Molodogvardeyskaya st., Samara, 443100, Russia

<sup>b</sup> All-Russian Research Institute of Oil Refining, 6/1 Aviamotornaya st., Moscow, 111116, Russia

## ARTICLE INFO

### Keywords:

Hydrodesulfurization  
Dibenzothiophene  
Unsupported catalysts  
Bulk MoS<sub>2</sub>

## ABSTRACT

Unsupported molybdenum disulfide catalysts were synthesized from ammonium tetrathiomolybdate with chitosan, hexadecylammonium and Triton X100 as structural agents by leaching of MoS<sub>2</sub>/Al<sub>2</sub>O<sub>3</sub> and MoS<sub>2</sub>/C/Al<sub>2</sub>O<sub>3</sub> catalyst supports with HF acid and covering of “FeS” seeds by the MoS<sub>2</sub> shell. Activation of the solids was performed under the H<sub>2</sub>S/H<sub>2</sub> flow or by the decomposition of precursors in the presence of a hydrocarbon solvent in an autoclave reactor with varied H<sub>2</sub> pressure. X-ray diffraction, N<sub>2</sub> adsorption, temperature-programmed reduction, X-ray photoelectron spectroscopy and transmission electron microscopy techniques were used to characterize their structure and morphology. The nature of organic additives and activation conditions affect the surface area, pore size distribution, and morphological characteristics of MoS<sub>2</sub> particles. Hydrodesulfurization of dibenzothiophene was performed in an autoclave reactor over unsupported MoS<sub>2</sub>-based catalysts. The catalytic behavior of bulk MoS<sub>2</sub> catalysts showed that the hydrogenation pathway prevailed over the direct desulfurization pathway. Higher HYD/DDS selectivity for dibenzothiophene hydrogenation was observed with the bulk molybdenum disulfide catalyst formed by etching of the MoS<sub>2</sub>/Al<sub>2</sub>O<sub>3</sub> catalyst support. Unsupported Mo sulfide catalysts exhibited high hydrogenation activity in dibenzothiophene hydrodesulfurization and, therefore, might find wide applications in hydropyrolysis of heavy feed and co-hydro-treating of petroleum fractions and plant oils.

## 1. Introduction

A removal of sulfur from oil fractions is necessary to minimize negative environmental impact of engine exhausts and to satisfy strict limitations on sulfur concentrations in fuels [1,2]. Stringent environmental standards require new catalysts with improved catalytic properties to achieve the 10–15 ppm sulfur content in motor fuels. Deep hydrodesulfurization (HDS) is especially challenging in the case of petroleum fractions with a high sulfur concentration close to 2–3 wt. %. The most common sulfur compounds in fuels are dibenzothiophene (DBT) and much less reactive alkyl-substituted DBTs such as 4,6-dimethylbenzothiophene (4,6-DMDBT) [3,4]. HDS usually proceeds through two pathways: a hydrogenation (HYD) route with aromatic ring hydrogenation and a hydrogenolysis route or direct desulfurization (DDS) pathway with a direct C–S bond cleavage [5]. The ratio of both pathways determines HYD/DDS selectivity and depends on the catalyst type. In the case of alkyl-substituted DBTs [6], steric hindrance of

methyl groups leads to hydrogenation of at least one aromatic ring before the elimination of sulfur. HDS of DBT in promoted Mo catalysts occurs mainly by the DDS route and a HYD/DDS ratio from 0.3 to 0.5. For that, it is necessary to develop catalysts with higher specific HYD activity.

Transition metal sulfide (TMS) hydrotreating catalysts are widely used in oil refineries for HDS, hydrodeoxygenation (HDO) and hydrodenitrogenation (HDN) reactions of petroleum feedstocks [7–9]. Conventional TMS HDS catalysts are usually supported on γ-Al<sub>2</sub>O<sub>3</sub> to ensure high active phase dispersion [7,10] and acceptable mechanical properties. The analysis of hydrotreating catalysts in last 80 years has shown that almost all opportunities to improve catalytic activity of supported Co(Ni)MoS catalysts reached the limit and the only way to enhance activity of TMS catalysts could be either increasing active phase loading or using bulk sulfides [11]. A new catalytic system NEBULA with a very high amount of the sulfide active phase without any support was developed by ExxonMobil and Albemarle. Such unsupported systems can

\* Corresponding author at: Samara State Technical University, 244, Molodogvardeyskaya st., Samara, 443100, Russia.

E-mail addresses: [p.a.nikulshin@gmail.com](mailto:p.a.nikulshin@gmail.com), [nikulshinpa@vniinp.ru](mailto:nikulshinpa@vniinp.ru) (P.A. Nikulshin).

be used for hydrotreatment (HDT) of not only light crudes but for heavy crudes either [12].

Heavy feedstock upgrading processes are carried out in harsh operating temperature (400–450 °C) and pressure (9–20 MPa) conditions with thermal cracking and catalytic hydrogenation and simultaneous removing of heteroatom compounds. There are several processes for conversion of heavy feeds into lighter ones using different technologies: hydrodesulfurization, delayed coking, LC-FINING, residue desulfurization, and solvent deasphalting. Unsupported molybdenum disulfide is utilized in the Eni Slurry Technology (EST) process and can be used for total feedstock conversion to distillates [13]. EST can process a broad variety of high-boiling feedstocks: heavy and extra-heavy oils, atmospheric and vacuum residues, visbroken tars, coal liquids, and bitumen from oil sands. A highly dispersed unsupported MoS<sub>2</sub> catalyst provides HYD activity and prevents an acid catalyst from rapid deactivation and coke formation under the process conditions. Conversion to lighter products is related to a thermal process whereas the presence of a dispersed catalyst and hydrogen allows avoiding coke formation [14]. HYD activity is also a very important step in HDS of low active compounds with a high steric effect such as alkyl substituted dibenzothiophenes, whose concentration in heavy feedstocks is extremely high. Developing of a new synthetic approach to production of high performance unsupported systems with high HYD activity is a promising research area. In terms of the above, the aim of this work was to prepare new catalysts by leaching of alumina and carbon-covered alumina MoS<sub>2</sub>/Al<sub>2</sub>O<sub>3</sub> and MoS<sub>2</sub>/C/Al<sub>2</sub>O<sub>3</sub> solids with HF acid and to compare their active phase species characteristics and DBT HDS properties with those obtained by well-known methods (via decomposition of ammonium tetrathiomolybdate [15] per se or in the presence of chitosan [16], hexadecylammonium or Triton X100 [17] as structural agents and with covering of “FeS” seeds by the MoS<sub>2</sub> shell [18]). Bulk MoS<sub>2</sub> obtained by traditional ammonium tetrathiosalts (NR<sub>4</sub>)<sub>2</sub>MoS<sub>4</sub> (R=H or alkyl group) thermal decomposition has low surface area due to MoS<sub>2</sub> particle sintering in the case of ATTM as precursor [15] or blocking of MoS<sub>2</sub> particles by carbon deposits from alkyl groups [17]. Consequently, bulk MoS<sub>2</sub> obtained by leaching with HF from a Al<sub>2</sub>O<sub>3</sub> or C/Al<sub>2</sub>O<sub>3</sub> should be free from such shortcomings.

## 2. Experimental

### 2.1. Preparation of catalysts

The preparation of catalysts was carried out by two steps. The first step was the synthesis of precursors in aqueous or mixed solutions. In the second step, the latter were activated by heating in the gas flow of 60 mL/min 15 vol. % H<sub>2</sub>S/H<sub>2</sub> with temperature increasing at a rate of 5 °C / min up to 400 °C and kept for 2 h. High-purity starting materials for the precursors were supplied by Sigma-Aldrich.

High-purity ammonium heptamolybdate was purchased from Sigma-Aldrich. Ammonium tetrathiomolybdate (NH<sub>4</sub>)<sub>2</sub>MoS<sub>4</sub> (ATTM) was first obtained by H<sub>2</sub>S bubbling in an aqueous solution of ammonium heptamolybdate for 5 h according to the standard procedure reported in [15]. The precipitated dark red crystals were filtered, washed with ethanol, dried, and stored in a refrigerator. The composition and structure of prepared crystals were confirmed by elemental analysis and XRD. Decomposition of ATTM was carried out in a quartz reactor. The quartz reactor was placed in a steel tube at the heating zone of a horizontal furnace. The resulting black powder after activation was labeled as Ref-MoS<sub>2</sub> and was used as the reference bulk MoS<sub>2</sub> catalyst synthesized without any additives.

Stainless steel 300 mL autoclaves were used for the synthesis. ATTM (1 g), 50 mL of hexadecane and 150 mL of water were put in each autoclave. Then the autoclaves were tightly sealed and maintained at 350 °C and under 4 or 14 MPa of hydrogen for 1 h. Two corresponding samples were denoted as 4-MoS<sub>2</sub> and 14-MoS<sub>2</sub>. After heating, the autoclaves were cooled naturally. The resulting black powder was filtered

and washed with water and acetone.

Several substances from different families of surfactants were tried as textural agents [19,20]. In a typical pre-catalyst preparation, 50 mL deionized water containing 6 g ATTM (0.023 mol) was added to a solution of 11.17 g of the nonionic surfactant Triton X114 and 14.91 g of hexadecylamine C<sub>16</sub>H<sub>36</sub>N. The resulting solution was transferred to the reactor and flushed with H<sub>2</sub> to remove any traces of oxygen. Then the autoclave was pressurized with hydrogen to 3.1 MPa (450 psi), stirred to 300 rpm and heated up to 623 K at 10 K/min and aged for 1 h. The resulting dark precipitate was separated by filtration and washed with acetone. The catalyst after activation was labeled as Trit-MoS<sub>2</sub>. The same synthesis was repeated with chitosan and the resulting catalyst was denoted Chit-MoS<sub>2</sub>.

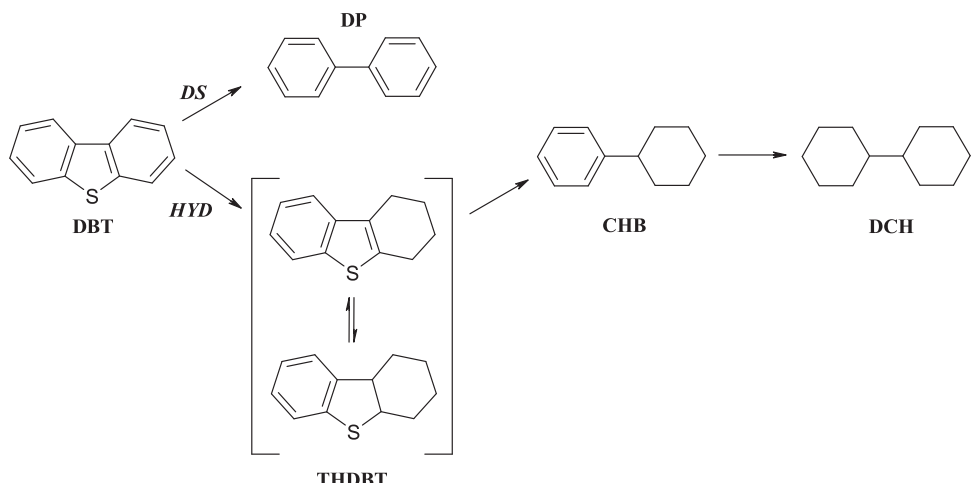
Core-shell MoS<sub>2</sub>/FeS bulk catalyst was prepared according to previously reported protocol [18] for Co<sub>9</sub>S<sub>8</sub>@MoS<sub>2</sub> system. However, due to possible spillover effect and ability of Co<sub>9</sub>S<sub>8</sub> particles to accelerate hydrogen dissociation as well as opportunity to form more active CoMoS sites, the Co<sub>9</sub>S<sub>8</sub> seeds were changed to more inert FeS ones. To prepare “FeS” seeds of the core-shell MoS<sub>2</sub>/FeS bulk catalyst 50 mL ammonium sulfide (20 wt. % of (NH<sub>4</sub>)<sub>2</sub>S in ammonium hydroxide) was added to a solution of Fe(NO<sub>3</sub>)<sub>3</sub>·9H<sub>2</sub>O in 50 mL of ethylene glycol. In the core-shell particle synthesis, 3.2 g elemental sulfur was added to 50 mL of ethylene glycol. The mixture was heated up to 196 °C under stirring for 1 h. Then, the solution of 1.75 g ammonium heptamolybdate in 50 mL ethylene glycol and the “FeS” seeds suspension were heated to 180 °C and added rapidly to the elemental sulfur solution. The reaction mixture was refluxed for 1 h and cooled to room temperature. The black powder was separated by filtration and washed with warm acetone to remove unreacted sulfur. The precursor of the core-shell MoS<sub>2</sub>/FeS catalyst was activated as usual.

$\gamma$ -Alumina was prepared by peptization of AlOOH boehmite TH60 (Germany, Sasol Company) with nitric acid and molding by extrusion. The extrudates were dried at 80, 100 and 110 °C for 2 h and calcined at 550 °C for 2 h. The carbon-coated support was synthesized by the pyrolysis of a mixture of iso-propanol with glycerol on alumina in a bench-scale flow reactor at 600 °C in the N<sub>2</sub> flow for 2 h. The carbon content in the carbon-coated support was set at 2 wt. % and controlled by the STA-TGA analysis. The precursors were prepared by the incipient wetness technique via impregnation of the support (Al<sub>2</sub>O<sub>3</sub> or C<sub>x</sub>/Al<sub>2</sub>O<sub>3</sub>) with aqueous solutions of 12-molybdophosphoric heteropolyacid H<sub>3</sub>PMo<sub>12</sub>O<sub>40</sub>·3H<sub>2</sub>O. The theoretical MoO<sub>3</sub> content in the precursor was 26 wt.%. Before the catalyst preparation, the pre-catalyst samples were activated by sulfidation in the gas flow of 60 mL/min 15 vol. % H<sub>2</sub>S/H<sub>2</sub> and at temperature of 400 °C for 4 h. A typical HF etching process was carried out as follows [21]. The 10 g sulfided MoS<sub>2</sub>/Al<sub>2</sub>O<sub>3</sub> or MoS<sub>2</sub>/C/Al<sub>2</sub>O<sub>3</sub> pre-catalyst, 193 g 45 wt. % HF, and 474 mL deionized water were added to a plastic beaker. The solution reacted for 4 h at 40 °C under vigorous stirring to form a black suspension. Next, the solid particles were separated by filtration and the supernatant fluid was discarded and neutralized with NaOH. The solid residue was washed with 50 mL deionized water and acetone. The activated catalysts were labeled as Et-MoS<sub>2</sub> and Et-MoS<sub>2</sub>/C, respectively.

### 2.2. Characterization of the catalysts

#### 2.2.1. Textural characteristics

Characterization of bulk catalysts was performed on samples obtained after catalytic experiments. The samples were separated from the reaction mixture by filtration, then washed with acetone to remove residual hydrocarbons and dried at room temperature. Specific surface areas were measured with an Autosorb-1 porosimeter by nitrogen adsorption at 77 K using the BET method. Prior to the measurements, the samples had been degassed under vacuum at 523 K for 2 h. Pore volume and pore size distributions in the mesopore domain were obtained from the adsorption branch of the isotherms and calculated by the Barrett-Joyner-Halenda (BJH) method at P/P<sub>0</sub> 0.99.



**Scheme 1.** Reaction network for the HDS of DBT: DBT – dibenzothiophene; THDBT – tetrahydrodibenzothiophene; DP – diphenyl; CHB – cyclohexylbenzene; DCH – dicyclohexyl.

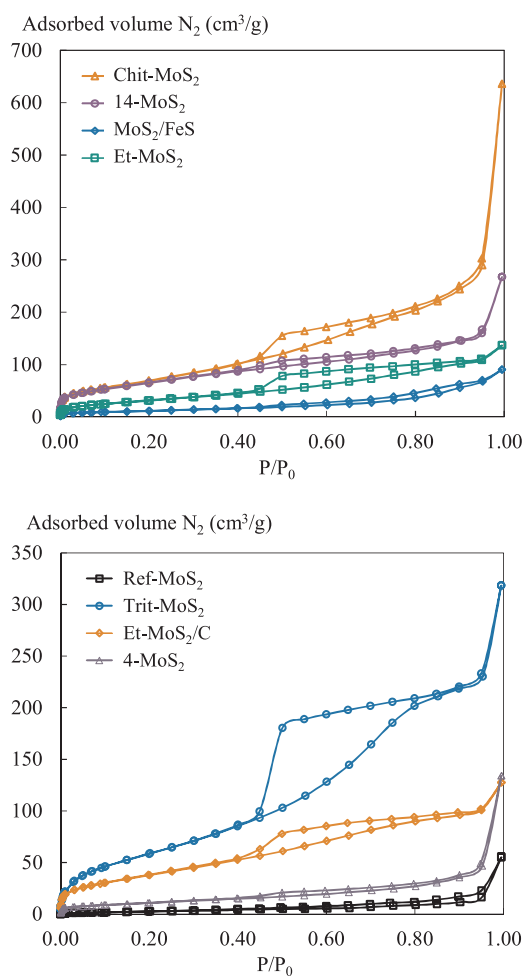


**Fig. 1.** Low-temperature nitrogen adsorption–desorption isotherms for the samples of bulk catalysts after catalytic test.

### 2.2.2. Temperature-programmed reduction (TPR)

Temperature-programmed reduction of the catalysts was carried out in a quartz reactor by two steps. At first, the samples were sulfided in the flow of  $\text{H}_2/\text{H}_2\text{S}$  (10 vol. %  $\text{H}_2\text{S}$ ) at 400 °C for 4 h. Secondary sulfided catalysts were subjected to temperature-programmed reduction with a mixture of  $\text{N}_2/\text{H}_2$  (5 vol. %  $\text{H}_2$ ) under the following conditions: a flow rate 25 mL/min, heating rate 10 °C/min, temperature range from 25 to

900 °C, and holding period 1 h at 900 °C. The TPR signals were detected using a thermal conductivity detector (TCD). Water produced in the course of TPR was adsorbed by granulated NaOH.

### 2.2.3. High-resolution transmission electron microscopy (HRTEM)

HRTEM was carried out on a Tecnai G2 20 electron microscope with 0.14 nm lattice-fringe resolution and accelerating voltage of 200 kV. The samples were prepared on a perforated carbon film mounted on a copper grid sample holder. 10–15 representative micrographs of each catalyst were visually examined and at least 500 slabs were handled to measure the key morphological characteristics.

The average slab length of  $\text{MoS}_2$   $\bar{L}$  was calculated as follows:

$$\bar{L} = \frac{\sum_{i=1..n} l_i}{n}, \quad (1)$$

where  $l_i$  is the length of slab  $i$ ,  $n$  is the total number of slabs. The average number of slabs per stack ( $\bar{N}$ ) was calculated as follows:

$$\bar{N} = \frac{\sum_{i=1..t} n_i \cdot N_i}{\sum_{i=1..t} n_i}, \quad (2)$$

where  $n_i$  is the number of stacks in  $N_i$  layers.

$\text{MoS}_2$  dispersion ( $D$ ) was statistically evaluated by dividing the total number of Mo atoms at the edge surface ( $Mo_e$ ), including corner sites ( $Mo_c$ ), by the total number of Mo atoms ( $Mo_T$ ) using the slab sizes measured in the TEM micrographs:

$$D = \frac{Mo_e + Mo_c}{Mo_T} = \frac{\sum_{i=1..t} 6n_i - 6}{\sum_{i=1..t} 3n_i^2 - 3n_i + 1}, \quad (3)$$

where  $n_i$  is the number of Mo atoms along one side of the  $\text{MoS}_2$  slab, as determined by its length, and  $t$  is the total number of slabs in the TEM micrograph.

### 2.2.4. X-ray diffraction (XRD)

XRD patterns were obtained on a ARLX'TRA diffractometer with  $\text{Cu K}_\alpha$  emission ( $\lambda = 1.54056 \text{ \AA}$ ) operating at 43 kV and 38 mA and identified using standard JCPDS files. Mean particles size was calculated using the Scherrer equation [22]:

$$d = \frac{k\lambda}{\beta \cos \theta}, \quad (4)$$

where  $d$  is the mean size of ordered (crystalline) domains ( $\text{\AA}$ );  $\lambda$  is the X-ray wavelength;  $\theta$  is the Bragg angle;  $\beta$  is the line broadening at half maximum intensity;  $k$  is the dimensionless shape factor. The shape factor  $k_{002}$  depends on the crystal shape and is close to 0.76 for  $\text{MoS}_2$

**Table 1**  
Composition and textural characteristics of synthesized catalysts.

Synthesis route	Catalyst designation	Specific surface area (m <sup>2</sup> /g)	Pore volume (cm <sup>3</sup> /g)	Content in the catalyst (wt. %)			S/Mo
				N	C	H	
Thermal decomposition of ATTM in H <sub>2</sub> S/H <sub>2</sub> flow at 400 °C	Ref-MoS <sub>2</sub>	11	0.09	0.4	1.1	0.07	1.8
Leaching of MoS <sub>2</sub> /Al <sub>2</sub> O <sub>3</sub> or MoS <sub>2</sub> /C/Al <sub>2</sub> O <sub>3</sub> catalysts with HF acid	Et-MoS <sub>2</sub>	121	0.21	0.3	2.2	0.61	1.8
	Et-MoS <sub>2</sub> /C	143	0.17	0.3	5.9	0.67	2.0
Decomposition of ATTM in autoclave at 4 or 14 MPa of H <sub>2</sub> pressure	4-MoS <sub>2</sub>	41	0.20	1.0	10.5	0.25	1.8
	14-MoS <sub>2</sub>	241	0.34	1.5	6.0	0.32	2.1
Hydrothermal decomposition of ATTM with chitosan or Triton X100	Trit-MoS <sub>2</sub>	231	0.54	2.4	31.3	0.65	2.0
Covering of “FeS” seeds by MoS <sub>2</sub> shell	Chit-MoS <sub>2</sub>	275	0.97	1.2	7.5	0.42	2.0
The incipient wetness impregnation of the supports with H <sub>3</sub> PMo <sub>12</sub> O <sub>40</sub> solution	MoS <sub>2</sub> /FeS	45	0.15	0.9	3.2	0.33	2.0
	MoS <sub>2</sub> /Al <sub>2</sub> O <sub>3</sub>	184	0.55	—	0.1	—	1.8
	MoS <sub>2</sub> /C/Al <sub>2</sub> O <sub>3</sub>	176	0.52	—	1.8	—	2.0

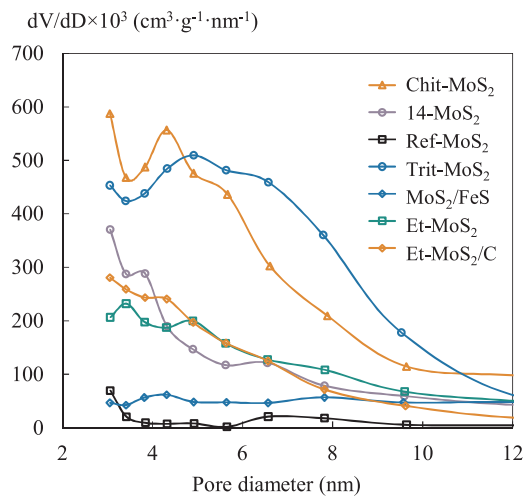


Fig. 2. The pore size distributions for bulk catalysts.

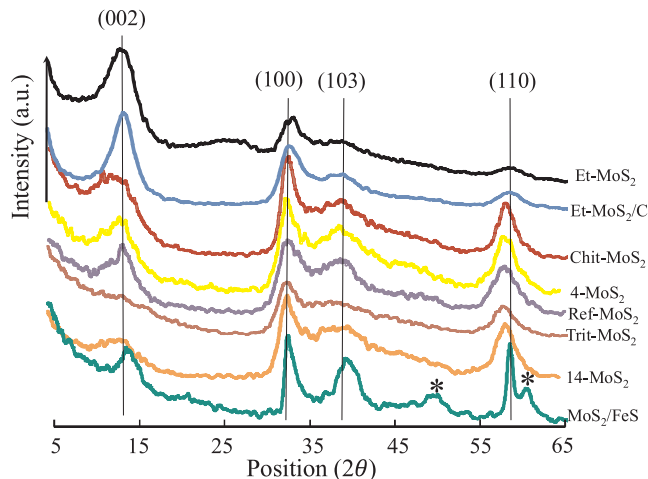


Fig. 3. XRD pattern of bulk MoS<sub>2</sub> catalysts. The (\*) shows FeS phase.

[23,24] The average number of layers  $\bar{N}$  was calculated using the equation  $\bar{N} = d_{002}/6.17$  ( $d_{002}$  in Å), where the value of the interlayer spacing in the 2H-MoS<sub>2</sub> structure corresponds to 6.17 Å.

#### 2.2.5. X-ray photoelectron spectroscopy (XPS)

The sulfided catalysts were analysed by XPS. The spectra were obtained on a Kratos Axis Ultra DLD spectrometer using a monochromatic AlK<sub>a</sub> source ( $h\nu = 1486.6$  eV, 150 W). The binding energy (BE) scale of the spectrometer was preliminarily calibrated using the position of the peaks for the Au 4f<sub>7/2</sub> (83.96 eV) and Cu 2p<sub>3/2</sub> (932.62 eV) core levels

of pure metallic gold and copper. The samples were mounted on a holder using double-sided adhesive tape. For the non-conductive samples, the Kratos charge neutraliser system was used and the spectra were charge-corrected to provide the C 1s spectral component of adventitious carbon (C–C, C–H) at 284.8 eV. In addition to the survey photoelectron spectra, narrow spectral regions (Al 2p, S 2p, Mo 3d, C 1s and O 1s) were recorded. The pass energy of the analyzer was 160 eV for the survey spectra and 40 eV for the narrow scans. The individual spectral regions were analyzed to determine the BE of the peaks, identify the chemical state of the elements and calculate the relative ratios of the elements on the catalyst surface.

The collected spectra were analysed using the CasaXPS software program (Version 2.3.16) after applying a Shirley background subtraction. Gaussian (30%)–Lorentzian (70%) peaks were used for spectra decomposition. The decompositions of the S 2p and Mo 3d XPS spectra were performed using the appropriate oxide and sulfided references as supported monometallic catalysts [25,26].

#### 2.3. Catalytic experiments

HDS of DBT was carried out in a R-201 high-pressure batch reactor (300 mL) equipped with a magnetically driven turbine which helps prevent the vortex formation and allows good gas dispersion in the liquid phase. The catalysts (0.25 g) were activated under H<sub>2</sub>S/H<sub>2</sub> (15% (v/v) H<sub>2</sub>S) at 673 K for 4 h and transferred to the reactor with the reactant mixture (0.86 wt. % of DBT in decane, 1 wt. % hexadecane as internal standard, total volume: 150 mL) without contact with the air. Before the reaction, the system had been flushed with H<sub>2</sub> to remove any oxygen traces. The autoclave was pressurized with hydrogen to 3.1 MPa (450 psi) and heated up to 573 K at 10 K/min. The stirring speed was kept at 300 rpm. At these conditions and stirring rate, the system was free of external mass transfer limitations. Once at 573 K, the reaction was monitored for 6 h by analyzing the samples using a Chromatec-Crystal gas chromatograph equipped with an OV-101 packed column to determine conversion versus time. The samples were taken every 20 min during the first hour, then every 30 min over the next five hours. The identity of the reaction products was confirmed by mass spectrometry with a Shimadzu GCMS-QP2010 Ultra.

The main reaction products in HDS of DBT were diphenyl (DP), formed by the so-called direct desulfurization pathway (DS), and cyclohexylbenzene (CHB) formed by initial hydrogenation (HYD) of one of the DBT aromatic rings. The HYD/DS selectivity ratio was evaluated from the product concentration ratio according to the reaction network for DBT HDS (Scheme 1):

$$S_{\text{HYD/DS}} = \frac{k_{\text{HYD}}}{k_{\text{DS}}} = \frac{C_{\text{CHB}} + C_{\text{DCH}}}{C_{\text{DP}}}, \quad (5)$$

where  $C_{\text{CHB}}$ ,  $C_{\text{DCH}}$  and  $C_{\text{DP}}$  are CHB, DCH and DP concentrations (wt. %) in the reaction products, respectively. The concentration of tetrahydrodibenzothiophene (THDBT), an intermediate hydrogenated

**Table 2**Morphological characteristics of the MoS<sub>2</sub> phase species calculated from TEM micrographs and XRD.

Catalyst	Average length $\bar{L}$ (nm)		Average stacking number $\bar{N}$		Distribution of slab length (rel. %)						Distribution of stacking number (rel. %)			
	HRTEM <sup>a</sup>	XRD <sup>b</sup>	HRTEM <sup>a</sup>	XRD <sup>b</sup>	< 2 nm	2–4 nm	4–6 nm	6–8 nm	8–10 nm	> 10 nm	1	2	3	> 4
Ref-MoS <sub>2</sub>	3.9	7.0	2.9	4.0	21	39	23	10	3	4	23	19	20	38
Et-MoS <sub>2</sub>	5.3	4.5	3.7	2.5	6	33	33	14	7	7	0	10	25	65
Et-MoS <sub>2</sub> /C	6.4	5.2	3.8	3.0	0	24	22	19	13	22	0	15	28	57
4-MoS <sub>2</sub>	11.3	6.4	4.1	3.0	0	1	5	8	20	67	0	0	10	90
14-MoS <sub>2</sub>	5.4	7.5	2.7	4.7	10	32	31	12	6	9	9	33	26	32
Trit-MoS <sub>2</sub>	14.4	6.6	3.8	—	0	1	1	6	8	83	0	8	21	71
Chit-MoS <sub>2</sub>	—	9.0	—	2.9	—	—	—	—	—	—	—	—	—	—
MoS <sub>2</sub> /FeS	22.4	22.8	3.1	3.7	0	2	3	11	6	77	0	3	23	75
MoS <sub>2</sub> /Al <sub>2</sub> O <sub>3</sub>	4.7	—	2.0	—	5	35	39	21	—	—	35	53	10	2
MoS <sub>2</sub> /C/ Al <sub>2</sub> O <sub>3</sub>	5.3	—	2.6	—	2	36	48	14	—	—	20	58	18	4

<sup>a</sup> Obtained from TEM analysis and calculation according Eqs. (1) and (2).<sup>b</sup> Obtained from XRD analysis using the Scherrer Eq. (4).

product also formed along the HYD pathway, remained low and could be neglected when calculating the HYD/DS ratio. Catalytic activity was defined in terms of DBT conversion (%) as a function of reaction time.

The rate constant of pseudo-first-order reactions of DBT HDS was determined by the equation:

$$k_{\text{HDS}} = -\frac{m_{\text{DBT}}}{m_{\text{cat}} \cdot t} \ln(1 - x_{\text{DBT}}), \quad (6)$$

where  $k_{\text{HDS}}$  is pseudo-first-order reaction constants for DBT HDS ( $\text{s}^{-1}$ ),  $x_{\text{DBT}}$  is conversions (%) of DBT,  $t$  is contact time (s), and  $m_{\text{DBT}}$  and  $m_{\text{cat}}$  are DBT weight (g) and weight of the catalyst (g), respectively.

Turnover frequencies (TOF,  $\text{s}^{-1}$ ) normalised on edge sites of MoS<sub>2</sub> slabs for DBT HDS allowed a deeper understanding of the catalytic properties of the active phase species. TOF values were calculated by the equation:

$$\text{TOF}_{\text{HDS}} = \frac{n_{\text{DBT}} \cdot x_{\text{DBT}}}{n_{\text{Mo}} \cdot t \cdot D}, \quad (7)$$

where  $t$  is contact time,  $x_{\text{DBT}}$  is conversions (%) of DBT at  $t$ ,  $n_{\text{DBT}}$  is the DBT amount (mol),  $D$  is MoS<sub>2</sub> species dispersion calculated by Eq. (3).

### 3. Results

#### 3.1. Physicochemical properties of the synthesized catalysts

The prepared bulk catalysts differ from each other in textural characteristics depending on the synthetic method and activation conditions. Low-temperature nitrogen adsorption–desorption isotherms for the bulk catalyst samples after the catalytic tests are presented in Fig. 1. Mesostructures of the bulk samples characteristically exhibit type IV isotherms with a little or zero additional uptake at high N<sub>2</sub> partial pressures [27]. The hysteresis loop area and quantity of adsorbed N<sub>2</sub> increased significantly for the Trit-MoS<sub>2</sub> sample (Fig. 1). Different additives and treatment under varying conditions yielded catalysts with variable crystallinity and textural characteristics. Surfactant additives used in the precursor had an important effect on the total pore volume and the surface area of the bulk MoS<sub>2</sub> catalysts. For 4-MoS<sub>2</sub> and MoS<sub>2</sub>/FeS solids, a very poorly developed porous system was observed with the surface area of only 41 and 45 m<sup>2</sup>/g, respectively (Table 1). Decomposition of ATT in the autoclave at different H<sub>2</sub> pressures shows that a pressure increase leads to significant growth of the specific surface area. The pore size adsorption graphs revealed wide pore size distribution in a mesopore range with no clear maxima (Fig. 2). Table 1 summarizes specific surface areas and pore volumes of different bulk MoS<sub>2</sub> catalysts. The specific surface area varied from minimal – 11 m<sup>2</sup>/g for the Ref-MoS<sub>2</sub> catalyst to maximal – 275 m<sup>2</sup>/g for Chit-MoS<sub>2</sub>. Use of organic additives [15] allows to achieve high specific surface area

because the carbon prevents the sintering of the MoS<sub>2</sub> particles during the thermal activation of the catalyst and participates in the formation of the porous catalyst surface. The sintering of carbon particles and molybdenum disulfide during the thermal activation of precursors does not allow us to separate these two phases and determine the surface area of each phase separately. The pore volume also showed a broad range of values from 0.09 cm<sup>3</sup>/g for Ref-MoS<sub>2</sub> and 0.97 cm<sup>3</sup>/g for the Chit-MoS<sub>2</sub> catalyst.

The catalyst composition was identified by bulk elemental analysis (Table 1). The carbon content varied between 1.1 wt. % for the Ref-MoS<sub>2</sub> catalyst and 31.3 wt. % for the Trit-MoS<sub>2</sub> catalyst. The nitrogen content varied from 0.3 wt. % for Et-MoS<sub>2</sub> and 2.4 wt. % for Trit-MoS<sub>2</sub>. S/Mo ratio in prepared catalysts was varied between 1.8–2.1 that is close to stoichiometric value in MoS<sub>2</sub>.

Fig. 3 shows XRD patterns of the prepared bulks. The MoS<sub>2</sub> phase was only observed in all bulk catalysts by XRD (with the exception of the MoS<sub>2</sub>/FeS sample with the FeS phase peaks). The MoS<sub>2</sub> sample exhibited three well-resolved peaks at 14.4°, 33.5°, 40°, and 58.6°, which can be indexed as the 002, 100, 103, and 110 reflections of the 2D hexagonal structure (JCPDS 37-1492). The average stacking height of bulk MoS<sub>2</sub> was estimated by the Debye–Scherrer equation based on the full width at half maximum of the highest intensity peak of the MoS<sub>2</sub> (002) peak, as shown in Table 2.

The morphology, size and stacking number of crystallites in the sulfided catalysts were observed by HRTEM [28]. As an example, a few HRTEM images of the sulfided samples are shown in Fig. 4. It is known that MoS<sub>2</sub> is a layered phase with a hexagonal crystallographic structure and is seen as black thread-like lines in the HRTEM images. Indeed, the micrographs have their typical fringes. The HRTEM images of the bulk catalyst showed only the presence of randomly packed MoS<sub>2</sub> layer stacks. Statistical results of stacking layer number distributions and the length of MoS<sub>2</sub> slabs of the bulk and supported catalysts are given in Table 2. The lowest average length of 4.5 nm was determined for the Et-MoS<sub>2</sub> catalyst; the other studied etched catalyst Et-MoS<sub>2</sub>/C had higher average length of 5.2 nm, which in agreement with the characteristics of MoS<sub>2</sub> particles in supported precursors. The maximum average stacking number of 5.8 was found for the Trit-MoS<sub>2</sub> catalyst. The reference Ref-MoS<sub>2</sub> catalyst was characterized by the relatively long length and high average stacking number equal to 7.0 nm and 4.0, respectively. The use of organic additives led to an increase of the average length for Chit-MoS<sub>2</sub> and an increase of the average stacking number for Trit-MoS<sub>2</sub>.

TPR profiles of the sulfided bulk catalysts are shown in Fig. 5. The first reduction peak at 150–340 °C corresponds to reduction of S<sub>2</sub><sup>2-</sup> groups from the edges of MoS<sub>2</sub> slabs [29,30]. Areas of the reduction peaks differentiate much suggesting different hydrogen consumption. TPR profiles also show that peak maxima positions were affected by the

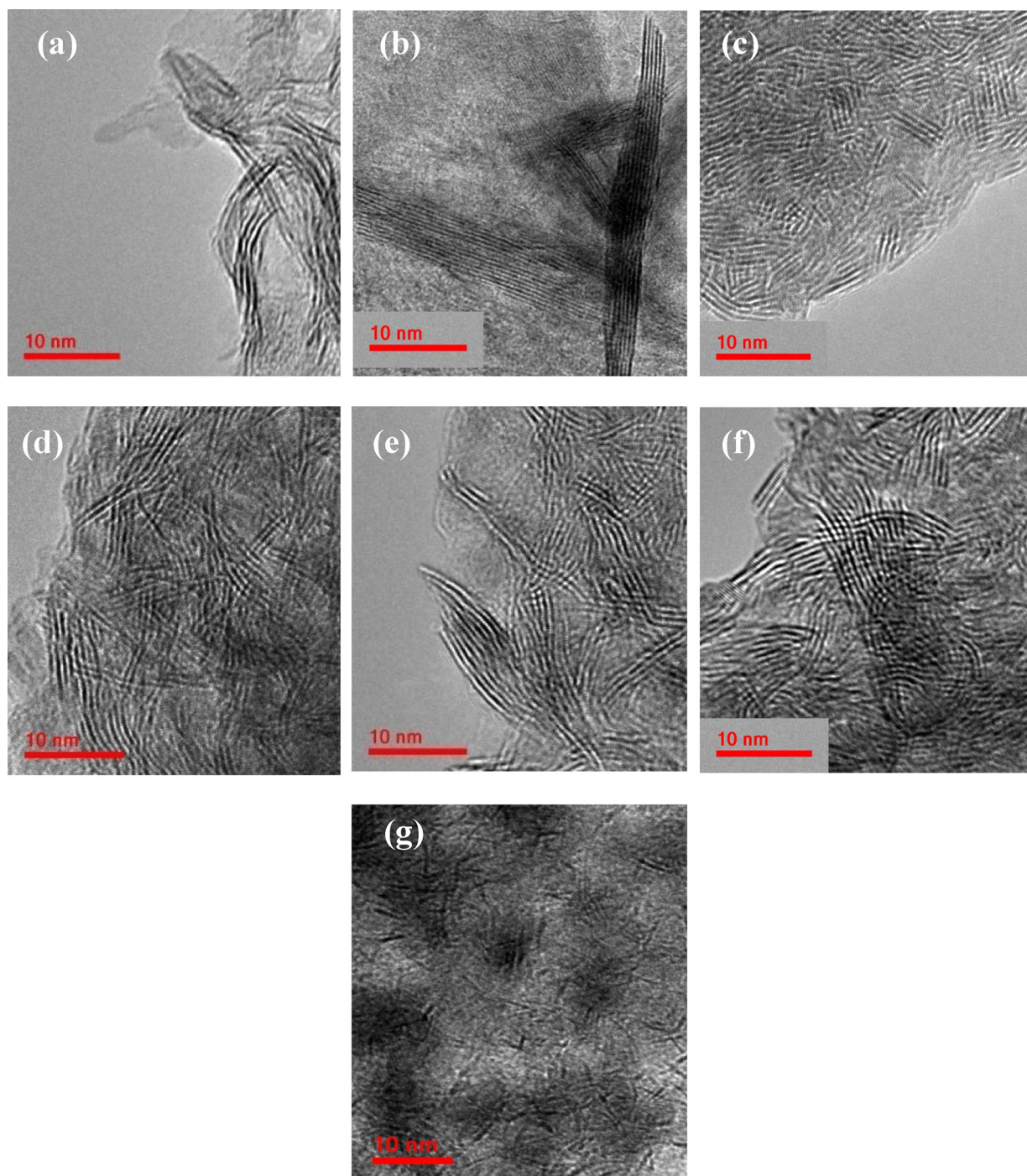


**Fig. 4.** Transmission electron micrographs of MoS<sub>2</sub> bulk catalysts: Trit-MoS<sub>2</sub> (a), MoS<sub>2</sub>/FeS (b), Ref-MoS<sub>2</sub> (c), 14-MoS<sub>2</sub> (d), 4-MoS<sub>2</sub> (e), Et-MoS<sub>2</sub> (f), Et-MoS<sub>2</sub>/C (g).

structure and synthesis route of the bulk MoS<sub>2</sub> catalyst. The TPR peaks in the 165–200 °C temperature region revealed that reduction temperatures for almost all catalysts (with the exception of the Chit-MoS<sub>2</sub> sample and MoS<sub>2</sub>/FeS) did not differ significantly. For the Chit-MoS<sub>2</sub> catalyst, the main peak was observed at 232 °C indicating that reducibility of Chit-MoS<sub>2</sub> and was lower than that of other catalysts. The highest TPR peaks (286 and 332 °C) were observed for MoS<sub>2</sub>/FeS solid. The lowest temperature ca. 165 °C was observed for Trit-MoS<sub>2</sub> and Et-MoS<sub>2</sub>. The TPR curves of the prepared catalysts have no shoulder at low temperature associated with reduction of more reactive active sites and, consequently, MoS<sub>2</sub> slabs have uniform center distribution.

More detailed information about the nature of the species formed after catalyst activation was obtained by XPS analysis. Fig. 6 shows

examples of the decomposition of Mo 3d photoelectron spectra recorded for the MoS<sub>2</sub>-based bulk catalysts as well as for the alumina and C-coated alumina supported references. The Mo 3d spectra contain three Mo 3d doublets: the doublet with binding energies at ca. 229.5 and 232.5 eV is associated to Mo<sup>4+</sup> species of the MoS<sub>2</sub> phase, the doublet with binding energies at 230.5 and 233.5 eV to Mo<sup>5+</sup> species of a MoS<sub>x</sub>O<sub>y</sub> oxysulfide species, and finally the doublet with binding energies at 232.5 and 235.6 eV to Mo<sup>6+</sup> oxide species. The decomposition of S 2s photopeaks presented two contributions assigned to sulfide (226.0 eV) and (S<sub>2</sub>)<sup>2-</sup> entities (227.5 eV). The S 2p core level spectrum exhibits a single S 2p3/2 contribution at 162.3 eV characteristic of S<sup>2-</sup> sulfur species.

The results of the XPS spectra decomposition revealed the metal

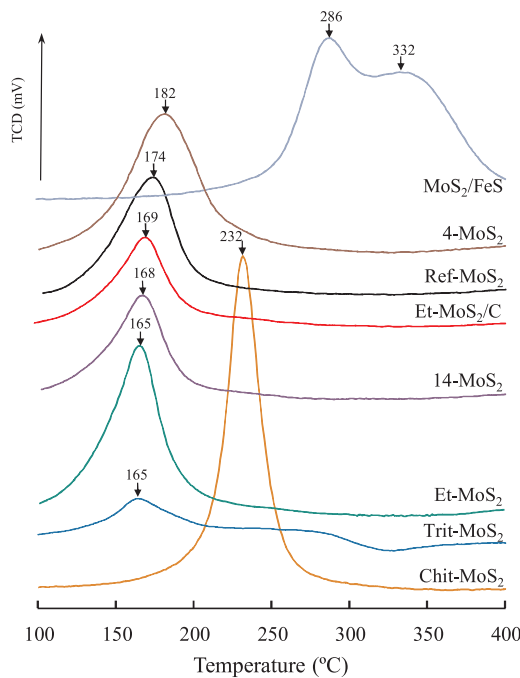


Fig. 5. TPR pattern of bulk  $\text{MoS}_2$  catalysts.

fractions of molybdenum species present on the surface of the sulfided  $\text{MoS}_2$ -based catalysts, summarized in Table 3. The S/Mo atomic ratios for all samples are close to the theoretical value of 2.0 expected for  $\text{MoS}_2$ . Etching of alumina by HF leads to formation of the solids in which almost all molybdenum presents in sulfide state (93–95%). Obviously, that part of Mo species present in oxide states in initial supported samples ( $\text{MoS}_2/\text{Al}_2\text{O}_3$  and  $\text{MoS}_2/\text{C}/\text{Al}_2\text{O}_3$ ) was dissolved during HF treatment as well as phosphorus that was absent in final unsupported sulfides. Trit- $\text{MoS}_2$  and  $\text{MoS}_2/\text{FeS}$  catalysts had a little lower  $\text{MoS}_2$  contribution that can be explained by using less severe conditions for their preparation.

A shift to lower binding energies at 0.4–0.5 eV for Mo 3d 5/2 and S 2p3/2 for Et- $\text{MoS}_2/\text{C}$  and  $\text{MoS}_2/\text{FeS}$  samples was also observed. Earlier Nogueira et al. [31] reported that these BE shifts can be caused by the residual presence of carbon species in strong interaction with  $\text{MoS}_2$ .

### 3.2. Catalytic activity in DBT HDS

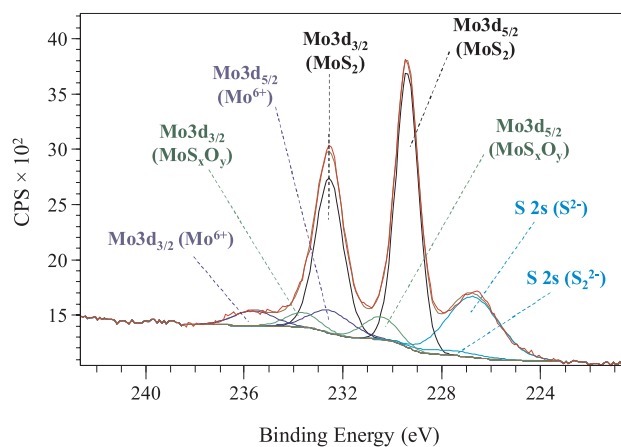
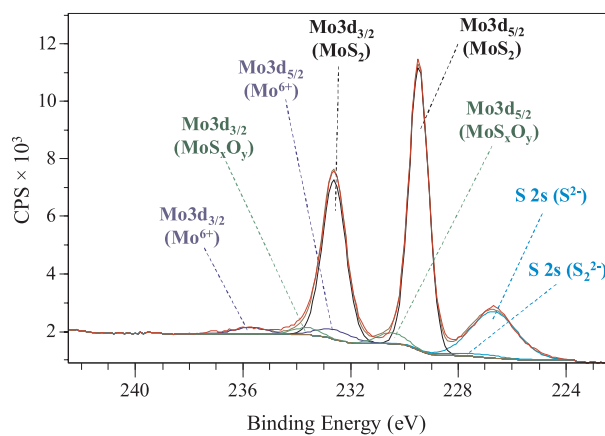
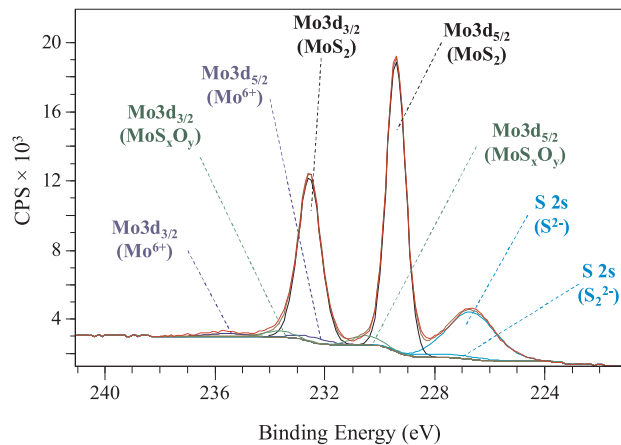
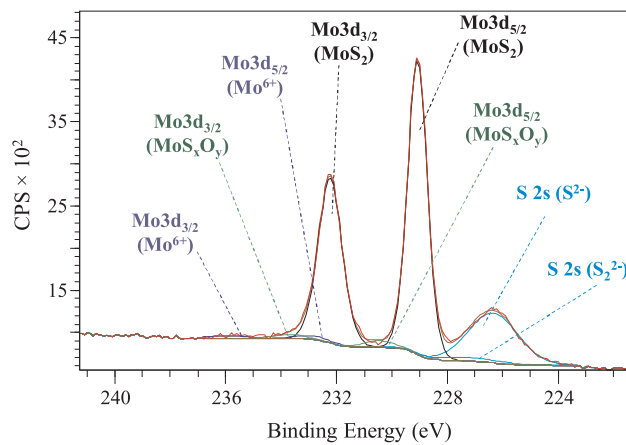
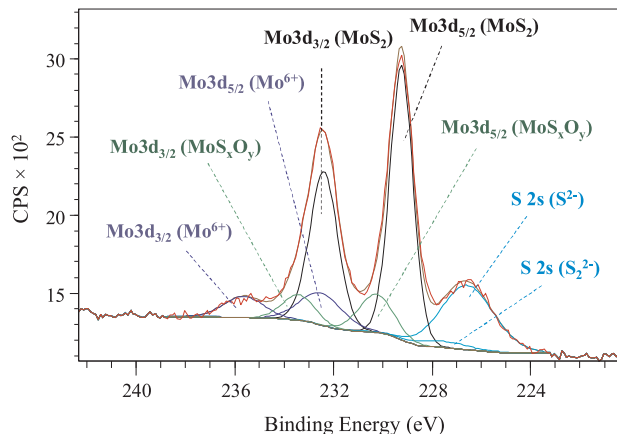
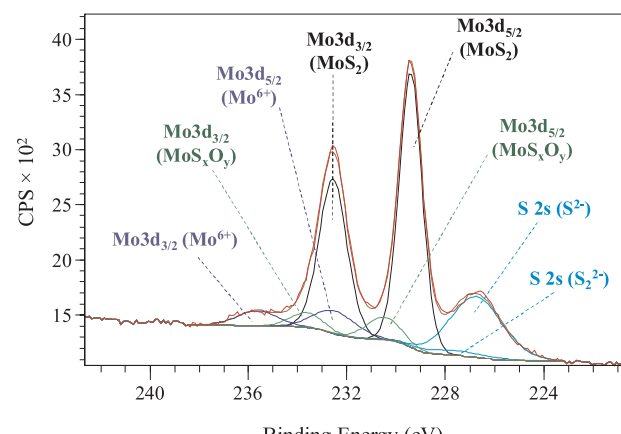
Catalytic activity of the bulk  $\text{MoS}_2$  catalyst was investigated in HDS of DBT at 573 K under hydrogen pressure of 3.1 MPa. Table 4 summarizes activity and selectivity values for all bulk catalysts. The rate constant of DBT HDS over the bulk catalysts varied from minimum  $0.35 \times 10^{-4} \text{ s}^{-1}$  ( $\text{MoS}_2/\text{FeS}$  catalyst) to  $2.98 \times 10^{-4} \text{ s}^{-1}$  (Et- $\text{MoS}_2$  catalyst). The Chit- $\text{MoS}_2$  catalyst had the lower TOF value in DBT HDS (TOF was  $9.6 \times 10^{-4} \text{ s}^{-1}$ ). The maximum TOF number was observed for the 4- $\text{MoS}_2$  catalyst. The selectivity ratio  $S_{\text{HYD/DS}}$  reported in Table 4 for all bulk catalysts varied between 1.0 and 4.5 at 10% conversion and between 1.9 and 7.2 at 30% conversion. The  $S_{\text{HYD/DS}}$  selectivity factor of all samples was much higher than 1.0, what means that HYD is more preferable than DS and, consequently, cyclohexylbenzene and dicyclohexyl are the major products of DBTHDS. It can be seen that 14- $\text{MoS}_2$ , Et- $\text{MoS}_2$  and Et- $\text{MoS}_2/\text{C}$  catalysts showed higher HDS activity and selectivity for the hydrogenation pathway (HYD) (Scheme 1). It should be noticed that  $S_{\text{HYD/DS}}$  values for prepared bulk  $\text{MoS}_2$ -based catalyst were much higher than those for supported  $\text{MoS}_2/\text{Al}_2\text{O}_3$  and  $\text{MoS}_2/\text{C}/\text{Al}_2\text{O}_3$  ones.

### 4. Discussion

A TPR analysis had been previously used for the sulfided catalysts to provide a measure of chemical reactivity [32]. Hydrogen consumption was defined by centers on the  $\text{MoS}_2$  species responsible for the formation of an anion vacancy, which is subsequently correlated to a catalytic active site [33]. Lower temperatures of the first reduction peaks were observed on the Et- $\text{MoS}_2$  and Et- $\text{MoS}_2/\text{C}$  catalysts. It means that such catalysts possess more labile sulfur atoms (low strength of the Mo–S bond [29] and, consequently, more reactive active sites). Higher temperatures were found for  $\text{MoS}_2/\text{FeS}$  and Chit- $\text{MoS}_2$ . The 3D shape surface (Fig. 7) was formed by a dependence of the temperature maximum of the first reduction peak and the amount of consumed  $\text{H}_2$  correlated with catalytic activity in DBT HDS and the carbon and nitrogen content in bulk  $\text{MoS}_2$  systems. According to Fig. 7, catalytic activity increased with the decrease of the strength (reduction  $T_{\max}$ ) and content (amount of consumed  $\text{H}_2$ ) of the active site. Also, catalytic activity strongly depends on the carbon content, especially for catalysts with low temperature area centers (14- $\text{MoS}_2$  and Trit- $\text{MoS}_2$ ). Higher catalytic activity of Ref- $\text{MoS}_2$  and Et- $\text{MoS}_2$  catalysts can be attributed to the high content of active sites with more labile sulfur atoms (the area of reduction temperature during TPR lower than 180 °C). The 14- $\text{MoS}_2$  catalyst placed close to them had low activity due to the higher amount of carbon (6.0 wt. %) and nitrogen (1.5 wt. %). Some lower activity of Et- $\text{MoS}_2/\text{C}$  located in the same reduction temperature area was caused by the lower amount of active centers (the amount of consumed  $\text{H}_2$  lower than 100  $\mu\text{mol/g}$ ) and higher carbon content (5.9 wt. %). However, the most negative influence of carbon and nitrogen was found for the Trit- $\text{MoS}_2$  catalyst.  $\text{MoS}_2/\text{FeS}$ , 14- $\text{MoS}_2$  and Chit- $\text{MoS}_2$  catalysts located in the area of  $\text{H}_2$  consumed in the amount of more than 400  $\mu\text{mol/g}$  had low  $k_{\text{HDS}}$  due to the strong S–Mo bond (high reduction temperature during TPR).

The most active catalysts (Et- $\text{MoS}_2$  and Et- $\text{MoS}_2/\text{C}$ ) had over 60% of the observed  $\text{MoS}_2$  particles with length shorter than 6.0 nm (Tables 2 and 4). Stacking layer number distributions (listed in Table 2) show that approximately 40% of the  $\text{MoS}_2$  slabs on the most active catalysts Et- $\text{MoS}_2$  and Et- $\text{MoS}_2/\text{C}$  contained from two to three layers, while catalysts Trit- $\text{MoS}_2$  and MoS<sub>2</sub>/FeS with low catalytic activity had more than 70% of  $\text{MoS}_2$  with four layers with poor dispersion.  $\text{MoS}_2/\text{FeS}$  sample has an amorphous FeS core structure, in contrast to the clearly visible core on TEM images of  $\text{Co}_9\text{S}_8@\text{MoS}_2$  [18]. The average particle length of curved  $\text{MoS}_2$  particles in  $\text{Co}_9\text{S}_8@\text{MoS}_2$  solid varied in the range 2–5 nm, while obtained  $\text{MoS}_2/\text{FeS}$  has extra long particles with average length 22.5 nm. The formation of high stack slabs results from the interaction between the support and Mo species. Basal-bonded  $\text{MoS}_2$  slabs could not be visualized while edge-bonded layers were visible [34]. HRTEM is capable of detecting less than 10% of the active phase. Nevertheless, HRTEM is still a valuable technique to get an overview of catalyst dispersion. Basing on that, the morphological characteristics were also determined by the XRD method (Table 2). The clear peak at 14.4° indicates significant  $\text{MoS}_2$  stacking. The (002) peak of sample Trit- $\text{MoS}_2$  cannot be integrated and the average stacking values were not derived from XRD. But (110) peak is quite clear and could be used to determine the average length by XRD. The broadening of the  $\text{MoS}_2$  peaks suggests the existence of nanoscale crystallites in different directions. Slight (002) peak shifts for sample Trit- $\text{MoS}_2$  is observed due to the rotation along the basal plane direction. XRD patterns were also used to determine the average  $\text{MoS}_2$  particle length and average number of layers  $\bar{N}$  (Table 2). The average stacking degree for bulk catalysts varied between 2.7 and 5.8 according to the Formula (4), which expectedly exceeded the values for conventional supported catalysts with 2–3 stacking layers [35]. For supported  $\text{MoS}_2/\text{Al}_2\text{O}_3$  and  $\text{MoS}_2/\text{C}/\text{Al}_2\text{O}_3$  catalysts, the average stacking degree and particle length were generally slightly lower compared to prepared bulk catalysts.

According to Fig. 7, the carbon and nitrogen content in bulk catalysts strongly impact catalytic activity. The presence of nitrogen in bulk

**MoS<sub>2</sub>/FeS****Trit-MoS<sub>2</sub>****Et-MoS<sub>2</sub>****Et-MoS<sub>2</sub>/C****MoS<sub>2</sub>/Al<sub>2</sub>O<sub>3</sub>****MoS<sub>2</sub>/C/Al<sub>2</sub>O<sub>3</sub>****Fig. 6.** XPS Mo 3d spectra recorded for MoS<sub>2</sub>-based bulk catalysts as well as MoS<sub>2</sub>/Al<sub>2</sub>O<sub>3</sub> and MoS<sub>2</sub>/C/Al<sub>2</sub>O<sub>3</sub> references.

catalysts could be explained by using nitrogen-containing ATTm as a precursor. Probably, the presence of ammonium during the synthesis process in autoclave reactor had led to the nitrogen incorporation into the MoS<sub>2</sub> crystallite and, as a result, inhibited activity in DBT HDS. The

catalytic activity decrease in the Chit-MoS<sub>2</sub> and 14-MoS<sub>2</sub> catalysts can be attributed to the high nitrogen amount. The carbon content also affected the specific surface area and activity of the MoS<sub>2</sub>-based catalysts (Fig. 8). Small carbon in the catalysts allowed to extend surface

**Table 3**

XPS analysis results of the unsupported MoS<sub>2</sub> samples and supported on Al<sub>2</sub>O<sub>3</sub> and C/Al<sub>2</sub>O<sub>3</sub> ones.

Catalyst	Binding energy (eV)		S/Mo at. ratio	P/Mo at. ratio	Contribution of MoS <sub>2</sub> (rel. %)
	Mo 3d <sub>5/2</sub>	S 2p <sub>3/2</sub>			
Ref-MoS <sub>2</sub>	229.5	162.4	2.0	—	100
Et-MoS <sub>2</sub>	229.4	162.3	2.0	—	93
Et-MoS <sub>2</sub> /C	229.1	161.9	2.0	—	95
Trit-MoS <sub>2</sub>	229.6	162.4	1.9	—	90
MoS <sub>2</sub> /FeS	229.1	161.9	2.1	—	86
MoS <sub>2</sub> /Al <sub>2</sub> O <sub>3</sub>	229.4	162.2	2.0	0.14	71
MoS <sub>2</sub> /C/ Al <sub>2</sub> O <sub>3</sub>	229.2	162.1	1.9	0.12	79

**Table 4**

Catalytic properties of MoS<sub>2</sub>-based catalysts in the HDS of DBT.

Catalyst	Selectivity ratio S <sub>HYD/DS</sub>		Rate constant k <sub>HDS</sub> × 10 <sup>4</sup> (s <sup>-1</sup> )	TOF values × 10 <sup>4</sup> (s <sup>-1</sup> )
	10% of conversion	30% of conversion		
Ref-MoS <sub>2</sub>	2.1	5.0	0.99 (± 0.04)	11.0 (± 0.4)
Et-MoS <sub>2</sub>	4.1	6.0	2.98 (± 0.1)	41.2 (± 1.4)
Et-MoS <sub>2</sub> /C	3.7	5.1	1.75 (± 0.05)	33.0 (± 1.1)
4-MoS <sub>2</sub>	3.4	4.0	1.46 (± 0.04)	48.5 (± 1.6)
14-MoS <sub>2</sub>	4.5	7.2	0.71 (± 0.02)	13.4 (± 0.4)
Trit-MoS <sub>2</sub>	2.0	3.3	0.54 (± 0.01)	35.4 (± 1.2)
Chit-MoS <sub>2</sub>	1.0	1.9	0.41 (± 0.06)	9.6 (± 0.3)
MoS <sub>2</sub> /FeS	2.1	3.2	0.35 (± 0.03)	16.5 (± 0.5)
MoS <sub>2</sub> / Al <sub>2</sub> O <sub>3</sub>	1.2	1.6	0.29 (± 0.01)	13.5 (± 0.2)
MoS <sub>2</sub> /C/ Al <sub>2</sub> O <sub>3</sub>	1.4	1.8	0.39 (± 0.01)	20.3 (± 0.3)

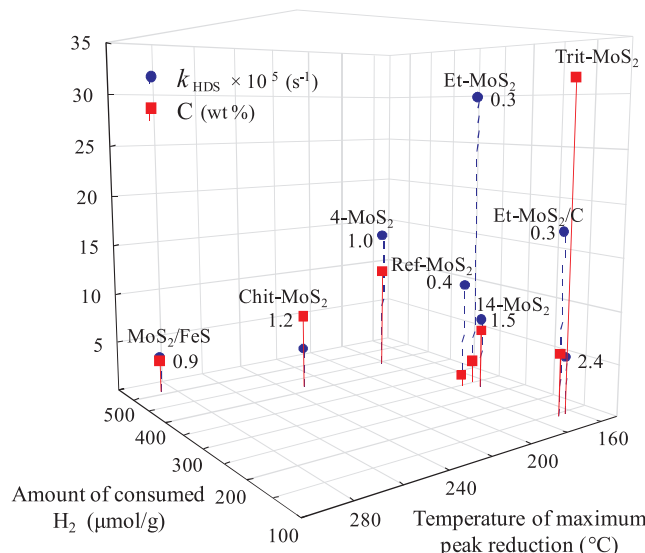


**Fig. 7.** 3D diagram for rate constant k<sub>HDS</sub> as a function of amount of consumed H<sub>2</sub> and reduction temperature during TPR analysis. (The values near the catalyst marker show the nitrogen content wt. %).

area and improve catalytic activity for 4-MoS<sub>2</sub> and Et-MoS<sub>2</sub>/C samples. Low activity of Trit-MoS<sub>2</sub> catalyst with high C-content was likely to be a consequence of limited access to active sites because of the carbon associated with MoS<sub>2</sub>.

The DBT in HDS reacts by two pathways: DS and HYD. The DS to HYD ratio depends on the catalyst properties and reaction conditions.

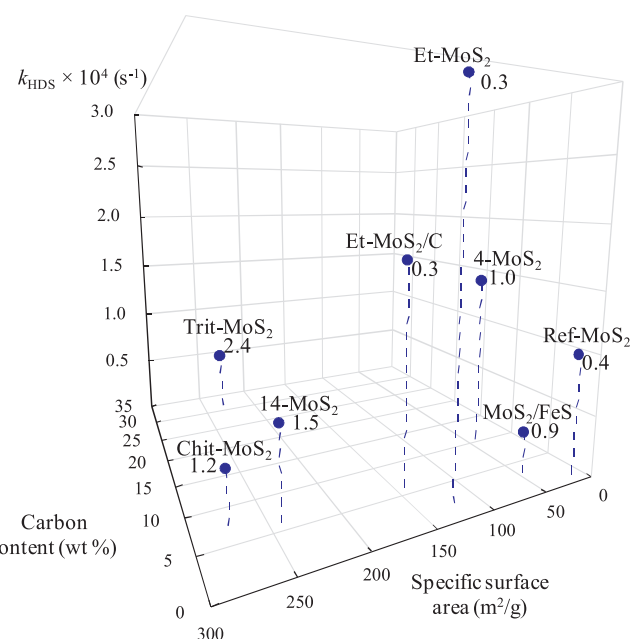


**Fig. 8.** 3D diagram for rate constant k<sub>HDS</sub> as a function of carbon content and specific surface area of the catalysts. (The values near the catalyst marker show the nitrogen content wt. %).

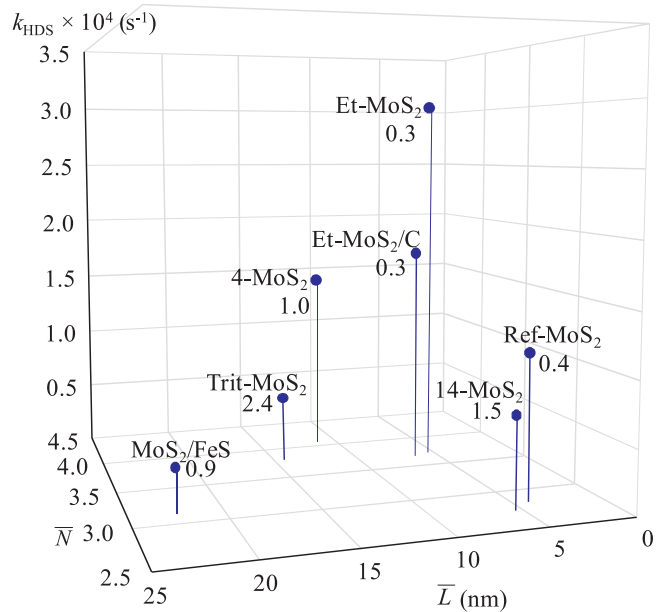


**Fig. 9.** 3D diagram for rate constant k<sub>HDS</sub> as a function of average length and average stacking number. (The values near the catalyst marker show the nitrogen content wt. %).

The DBT reaction pathways are shown in Scheme 1. It is clearly seen from Table 4 that the selectivity factor of the bulk catalysts increases with increasing reaction time due to the decrease in DS performance. Catalyst activity of the bulk MoS<sub>2</sub> solids was determined by the active phase morphology (Fig. 9). Higher activity corresponded to the Et-MoS<sub>2</sub> catalyst having the low average length and high stacking number. The dependence of S<sub>HYD/DS</sub> from the active phase morphology is shown in Fig. 10. Higher HYD/DS selectivity was achieved at minimal L and N. This relationship is in agreement with the “rim-edge” model [23,36], according to which HYD and DS sites have the same structure, albeit HYD sites are located on the rims whereas DS sites are located both on the rims and on the edges of the MoS<sub>2</sub> crystallite. The large total

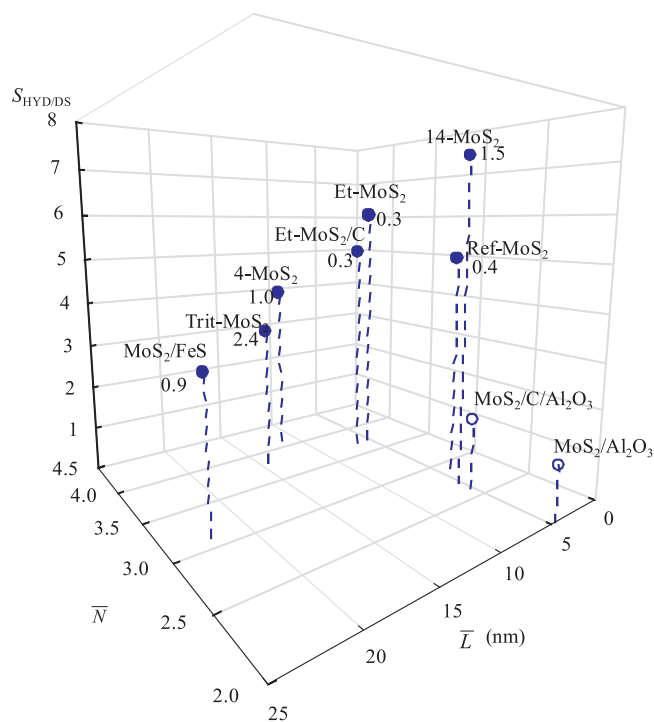


Fig. 10. 3D diagram for  $S_{\text{HYD/DS}}$  as a function of average length and average stacking number. (The values near the catalyst marker show the nitrogen content wt. %).

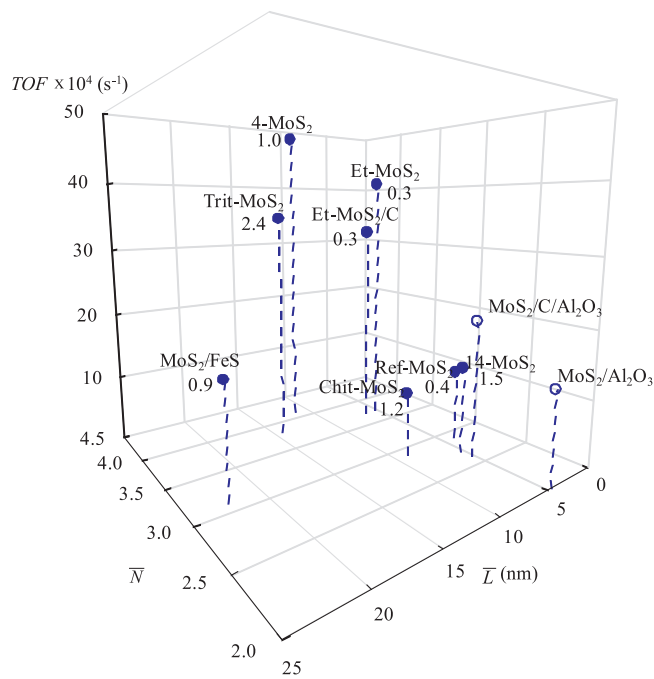


Fig. 11. 3D diagrams for TOF number as a function of average length and average stacking number. (The values near the catalyst marker (a) show the nitrogen content wt. %).

perimeter of the crystallites may result to the formation of a large number single Mo-sulfide sites located on the rims and responsible for HYD activity. It also may be a reason for high HYD selectivity because the number of DS sites in low-layered slabs might not be high [37]. Active sites on the spatial angles (at the edge and rim crossing) are highly coordinatively unsaturated and mostly responsible for HYD activity. The ratio of the crystallite diameter and height determines the

proportion of HYD and DS sites and hence catalyst selectivity in the HYD and DS reactions. Higher  $S_{\text{HYD/DS}}$  could be attributed to the high ratio of HYD sites on the spatial angles relatively to centers on the rim and edges due to the short slab and minimal average number of MoS<sub>2</sub> layers.

Rate constants  $k_{\text{HDS}}$  and TOF number for bulk and supported catalysts are summarized in Table 4. Rate constants for supported catalysts were 5–10 fold lower than those for their etched analogs. The TOF number was determined as the number of DBT molecules reacting at one active site per second and the TOF was calculated from the estimated rate constant and the initial DBT concentration. The TOF number for etched unsupported catalysts was 5–10 fold higher than that for supported Co(Ni)Mo/Al<sub>2</sub>O<sub>3</sub> systems. Fig. 10 shows the dependence of the TOF number in DBT HDS normalized on edge sites of MoS<sub>2</sub> slabs over the bulk and supported catalysts from the average length and average stacking number of the MoS<sub>2</sub> phase species. Catalysts with the higher stacking number, low size and nitrogen amount had maximal TOF values in DBT HDS (Fig. 11).

## 5. Conclusions

This study focused on the influence of the synthesis route and composition of bulk catalysts on HDS activity. The carbon and nitrogen content in bulk catalysts strongly affects catalytic activity. The nitrogen content of 2.4 wt. % was the highest for the catalysts prepared from the ammonium containing precursors in the autoclave. The high nitrogen content inhibits activity in DBT HDS, probably due to the nitrogen incorporation into the MoS<sub>2</sub> crystallite, and it follows that the most preferable way for the synthesis of bulk catalysts is support leaching from supported catalysts.

Unsupported molybdenum sulfide catalysts exhibited extremely high hydrogenation activity in HDS DBT being more than 2-fold higher than selectivity of Mo/Al<sub>2</sub>O<sub>3</sub> and Mo/C/Al<sub>2</sub>O<sub>3</sub> catalysts and 5-fold higher than selectivity of Co(Ni)Mo/Al<sub>2</sub>O<sub>3</sub> supported ones [38–40]. High HYD/DS selectivity of bulk catalysts may arise from the high ratio of HYD sites on spatial angles relative to centers on the rim and edges due to the short slab and minimal average number of MoS<sub>2</sub> layers.

The improved catalytic properties of the formed by support etching bulk MoS<sub>2</sub> catalysts might be extensively applied to hydroprocessing of heavy feed and co-hydrotreating of oil fractions and plant oil feedstocks.

## Acknowledgments

Authors thank Dr. K. Maslakov (Chemistry Department, M.V. Lomonosov Moscow State University) for XPS measurements. This research was financially supported by the Government of the Russian Federation (Decree No. 220 of April 9 2009) under the agreement No. 4.Z50.31.0038.

## References

- [1] I.V. Babich, J.A. Moulijn, Science and technology of novel processes for deep desulfurization of oil refinery streams: a review, *Fuel* 82 (2003) 607–631.
- [2] C. Song, An overview of new approaches to deep desulfurization for ultra-clean gasoline, diesel fuel and jet fuel, *Catal. Today* 86 (2003) 211–263.
- [3] U.T. Turaga, C. Song, Influence of nitrogen compounds on deep hydrodesulfurization of 4,6-dimethylbenzothiophene over Al<sub>2</sub>O<sub>3</sub>- and MCM-41-supported Co-Mo sulfide catalysts, *Catal. Today* 86 (2003) 265–275.
- [4] X. Ma, K. Sakanishi, I. Mochida, Three-stage deep hydrodesulfurization and decolorization of diesel fuel with CoMo and NiMo catalysts at relatively low pressure, *Fuel* 73 (1994) 1667–1671.
- [5] D.H. Broderick, B.C. Gates, Hydrogenolysis and hydrogenation of dibenzothiophene catalyzed by sulfide CoO-MoO<sub>3</sub>/γ-Al<sub>2</sub>O<sub>3</sub>; the reaction kinetics, *AIChE J.* 27 (1981) 663–673.
- [6] D.D. Whitehurst, T. Isoda, I. Mochida, Present state of the art and future challenges in the hydrodesulfurization of polycyclic aromatic sulfur compounds, *Adv. Catal.* 42 (1998) 345–471.
- [7] V.M. Kogan, P.A. Nikul'shin, V.S. Dorokhov, E.A. Permyakov, A.V. Mozhaev, D.I. Ishutenko, O.L. Eliseev, N.N. Rozhestvenskaya, A.L. Lapidus, Modern concepts

- on catalysis of hydroprocessing and synthesis of alcohols from syngas by transition metal sulfides, Russ. Chem. B+ 63 (2014) 332–345.
- [8] B. Delmon, Y.W. Li, Modelling of hydrotreating catalysis based on the remote control: HYD and HDS, J. Mol. Catal. Part A: Chem. 127 (1997) 163–190.
- [9] B.C. Gates, Catalytic Chemistry, Wiley, New York, 1992, p. 5.
- [10] H. Topsøe, B.S. Clausen, Active sites and support effects in hydrodesulfurization catalysts, Appl. Catal. 25 (1986) 273–293.
- [11] S. Eijsbouts, F. Plantenga, B. Lelieveld, Y. Inoue, K. Fujita, STARS and NEBULA—new generations of hydroprocessing catalysts for the production of ultra low sulfur diesel, Am. Chem. Soc. Div. Fuel Chem. 48 (2003) 494–495.
- [12] Y. Liu, L. Gao, L. Wen, Baoning Zong, Recent advances in heavy oil hydroprocessing technologies, Recent Pat. Chem. Eng. 2 (1) (2009) 22–36.
- [13] G. Bellussi, G. Rispoli, A. Landoni, R. Millini, D. Molinari, E. Montanari, D. Moscotti, P. Pollesel, Hydroconversion of heavy residues in slurry reactors: developments and perspectives, J. Catal. 308 (2013) 189–200.
- [14] N. Panariti, A. Del Bianco, G. Del Piero, M. Marchionna, P. Carniti, Petroleum residue upgrading with dispersed catalysts: part 2. Effect of operating conditions, Appl. Catal. A: Gen. 204 (2000) 215–222.
- [15] G. Alonso, J. Yang, M.H. Siadati, R.R. Chianelli, Synthesis of tetraalkyl ammonium thiometallates in aqueous solution, Inorg. Chim. Acta 325 (2001) 193–197.
- [16] F. Subhan, Production of ultra-low-sulfur gasoline: an equilibrium and kinetic analysis on adsorption of sulfur compounds over Ni/MMS sorbents, J. Hazard. Mater. 239–240 (2012) 370–380.
- [17] D. Genuit, I. Bezverkhy, P. Afanasiev, Solution preparation of the amorphous molybdenum oxysulfide MoOS<sub>2</sub> and its use for catalysis, Solid State Chem. 178 (2005) 2759–2765.
- [18] A. Hadj-Aissa, F. Dassenoy, C. Geanteta, P. Afanasiev, Solution synthesis of core-shell Co<sub>9</sub>S<sub>8</sub>@MoS<sub>2</sub> catalysts, J. Catal. Sci. Technol. 6 (2016) 4901–4909.
- [19] D. Genuit, P. Afanasiev, M. Vrinat, Solution syntheses of unsupported Co(Ni)–Mo–S hydrotreating catalysts, J. Catal. 235 (2005) 302–317.
- [20] Z. Le, P. Afanasiev, D. Li, X. Long, M. Vrinat, Solution synthesis of the unsupported Ni–W sulfide hydrotreating catalysts, Catal. Today 130 (2008) 24–31.
- [21] Y. Li, A. Li, F. Li, D. Liu, Y. Chai, C. Liu, Application of HF etching in a HRTEM study of supported MoS<sub>2</sub> catalysts, J. Catal. 317 (2014) 240–252.
- [22] M.P. De la Rosa, Structural studies of catalytically stabilized model and industrial-supported hydrodesulfurization catalysts, J. Catal. 225 (2004) 288–299.
- [23] M. Daage, R.R. Chianelli, Structure-function relations in molybdenum sulfide catalysts: the “Rim-Edge” model, J. Catal. 149 (1994) 414–427.
- [24] K.S. Liang, R.R. Chianelli, F.Z. Chien, S.C. Moss, Structure of poorly crystalline MoS<sub>2</sub>—a modeling study, J. Non-Cryst. Solids 79 (1986) 251–273.
- [25] P.A. Nikulshin, A.V. Mozhaev, K.I. Maslakov, A.A. Pimerzin, V.M. Kogan, Genesis of HDT catalysts prepared with the use of Co<sub>2</sub>Mo<sub>10</sub> HPA and cobalt citrate: study of their gas and liquid phase sulfidation, Appl. Catal. B 158–159 (2014) 161–174.
- [26] A.V. Mozhaev, P.A. Nikulshin, Al.A. Pimerzin, K.I. Maslakov, A.A. Pimerzin, Investigation of co-promotion effect in NiCoMoS/Al<sub>2</sub>O<sub>3</sub> catalysts based on Co<sub>2</sub>Mo<sub>10</sub>.
- heteropolyacid and nickel citrate, Catal. Today 271 (2016) 80–90.
- [27] Z. Zhang, T.J. Pinnavaia, Mesostructured γ-Al<sub>2</sub>O<sub>3</sub> with a lathlike framework morphology, J. Am. Chem. Soc. 124 (2002) 12294.
- [28] S. Eijsbouts, J.J.L. Heinerman, H.J.W. Elzerman, MoS<sub>2</sub> structures in high activity hydrotreating catalysts. II. Evolution of the active phase during the catalyst life cycle deactivation model, Appl. Catal. A: Gen. 105 (1993) 69–82.
- [29] B. Scheffer, N.J.J. Dekker, P.J. Mangnus, J.A. Moulijn, A temperature-programmed reduction study of sulfided CoMo/Al<sub>2</sub>O<sub>3</sub> hydrodesulfurization catalysts, J. Catal. 121 (1990) 31–46.
- [30] G.B. Mcgarvey, S. Kasztelan, An investigation of the reduction behavior of MoS<sub>2</sub>/Al<sub>2</sub>O<sub>3</sub> and the subsequent detection of hydrogen on the surface, J. Catal. 148 (1994) 149–156.
- [31] A. Nogueira, R. Znaigua, D. Uzio, P. Afanasiev, G. Berhault, Curved nanostructures of unsupported and Al<sub>2</sub>O<sub>3</sub>-supported MoS<sub>2</sub> catalysts: synthesis and HDS catalytic properties, Appl. Catal. 429–430 (2012) 92–105.
- [32] S.L. González-Cortés, T.C. Xiao, Costa PMFJ, B. Fontal, M.L.H. Green, Urea-organic matrix method: an alternative approach to prepare CoMoS<sub>2</sub>/γ-Al<sub>2</sub>O<sub>3</sub> HDS catalyst, Appl. Catal. A: Gen. 270 (2004) 209–222.
- [33] N.K. Nag, D. Fraenkel, J.A. Moulijn, B.C. Gates, Characterization of hydroprocessing catalysts by resolved temperature-programmed desorption, reduction and sulfiding, J. Catal. 66 (1980) 162–170.
- [34] J. Van Doorn, J.A. Moulijn, G. Djéga-Mariadassou, High-resolution electron microscopy of spent Ni–Mo/Al<sub>2</sub>O<sub>3</sub> hydrotreating catalysts, Appl. Catal. 63 (1990) 77–90.
- [35] M. Li, H. Li, F. Jiang, Y. Chu, H. Nie, The relation between morphology of (Co)MoS<sub>2</sub> phases and selective hydrodesulfurization for CoMo catalysts, Catal. Today 149 (2010) 35–39.
- [36] R.R. Chianelli, G. Berhault, B. Torres, Unsupported transition metal sulfide catalysts: 100 years of science and application, Catal. Today 147 (2009) 275–286.
- [37] P.A. Nikulshin, V.A. Salnikov, A.V. Mozhaev, P.P. Minaev, A.A. Pimerzin, Relationship between active phase morphology and catalytic properties of the carbon–alumina-supported Co(Ni)Mo catalysts in HDS and HYD reactions, J. Catal. 309 (2014) 386–396.
- [38] H. Liu, Y.P. Li, C.L. Yin, Y.L. Wu, Y.M. Chai, D.M. Dong, X.H. Li, C.G. Liu, One-pot synthesis of ordered mesoporous NiMo–Al<sub>2</sub>O<sub>3</sub> catalysts for dibenzothiophene hydrodesulfurization, Appl. Catal. B: Environ. 198 (2016) 493–507.
- [39] J.A. Toledo-Antonio, M.A. Cortes-Jacome, J. Escobar-Aguilar, C. Angeles-Chavez, J. Navarrete-Bolanos, E. Lopez-Salinas, Upgrading HDS activity of MoS<sub>2</sub> catalysts by chelating thioglycolic acid to MoO<sub>x</sub> supported on alumina, Appl. Catal. B: Environ. 213 (2017) 106–117.
- [40] C. Suresh, L. Pérez-Cabrera, J.N. Díaz de León, T.A. Zepeda, G. Alonso-Núñez, S. Fuentes Moyado, Highly active CoMo/Al (10) KIT-6 catalysts for HDS of DBT: role of structure and aluminum heteroatom in the support matrix, Catal. Today 296 (2017) 214–218.